

Supplementary Material

1 ADDITIONAL METHODS TO ESTIMATE SUBMARINE MELTWATER

1.1 Composite Tracer Method (CT)

To estimate submarine meltwater (SMW) fractions the CT method assumes mixing of 3 source waters: mCDW, WW, and SMW. The binary mixing lines among the 3 source waters construct a triangle and the deviation from the hypotenuse between mCDW and WW toward apex of SMW increases with the addition of SMW. Jenkins et al. (2018) defined the meltwater fraction (Φ) as the ratio of the distances from the hypotenuse to the observed values and to the properties of SMW source water as follow:

$$\Phi = \frac{(x_{obs}^2 - x_{mCDW}^2) - (x_{obs}^1 - x_{mCDW}^1)(x_{WW}^2 - x_{mCDW}^2)/(x_{WW}^1 - x_{mCDW}^1)}{(x_{SMW}^2 - x_{mCDW}^2) - (x_{SMW}^1 - x_{mCDW}^1)(x_{WW}^2 - x_{mCDW}^2)/(x_{WW}^1 - x_{mCDW}^1)}, \quad (S1)$$

where x^1 and x^2 are values of two chosen tracers. The potential temperature, salinity, and dissolved oxygen of mCDW, WW, and SMW were summarized in Table 1 of the main text.

1.2 $\delta^{18}\text{O}$ Method

The conservative property of $\delta^{18}\text{O}$ makes it a useful tracer of meteoric water, which includes glacial meltwater and precipitation, in polar region (Östlund and Hut, 1984). Sea ice meltwater (SIM) and mCDW are considered as source waters along with MET in Antarctic coastal oceans (Meredith et al., 2008; Randall-Goodwin et al., 2015). The system of linear equations is represented as follows:

$$\begin{aligned} f_{mCDW} + f_{MET} + f_{SIM} &= 1 \\ S_{mCDW} + S_{MET} + S_{SIM} &= S \\ \delta^{18}\text{O}_{mCDW} + \delta^{18}\text{O}_{MET} + \delta^{18}\text{O}_{SIM} &= \delta^{18}\text{O} \end{aligned} \quad (S2)$$

where f_{mCDW} , f_{MET} and f_{SIM} are the fractions of mCDW, SIM, and MET. The tracer properties of the source waters are presented in Table 1 of the main text. The average of the values >800 m at St. 9 – 11 was used for $\delta^{18}\text{O}$ of mCDW. $\delta^{18}\text{O}$ for MET and SIM were from Randall-Goodwin et al. (2015). For the calculation of meteoric water fractions with WW, instead of mCDW, as a source water (Figure 6 in the main text), the averages of the values at the depths of 100 – 400 m at Stations 7 and 8 were used for $\delta^{18}\text{O}$ and salinity of WW.

2 SUPPLEMENTARY TABLES AND FIGURES

Table S1. Uncertainties of source water properties. The properties for OMPA were perturbed within the uncertainty ranges for Monte Carlo simulation. Gas concentrations are in unit of mol kg⁻¹.

Source water	θ (°C)	S (psu)	³ He (10 ⁻¹⁵)	⁴ He (10 ⁻⁹)	Ne (10 ⁻⁹)	Ar (10 ⁻⁵)	Kr (10 ⁻⁹)	Xe (10 ⁻¹⁰)
AASW	0.53	0.12	0.063	0.037	0.152	0.0259	0.045	0.073
SMR	2	0.01	0.025	0.025	0.204	0.1090	0.322	0.643
SMW	4	0.01	5.493	3.970	13.77	0.7080	0.864	0.660
pWW	0.002	0.004	0.042	0.029	0.089	0.0068	0.016	0.026
mCDW	0.072	0.025	0.025	0.013	0.068	0.0068	0.029	0.051

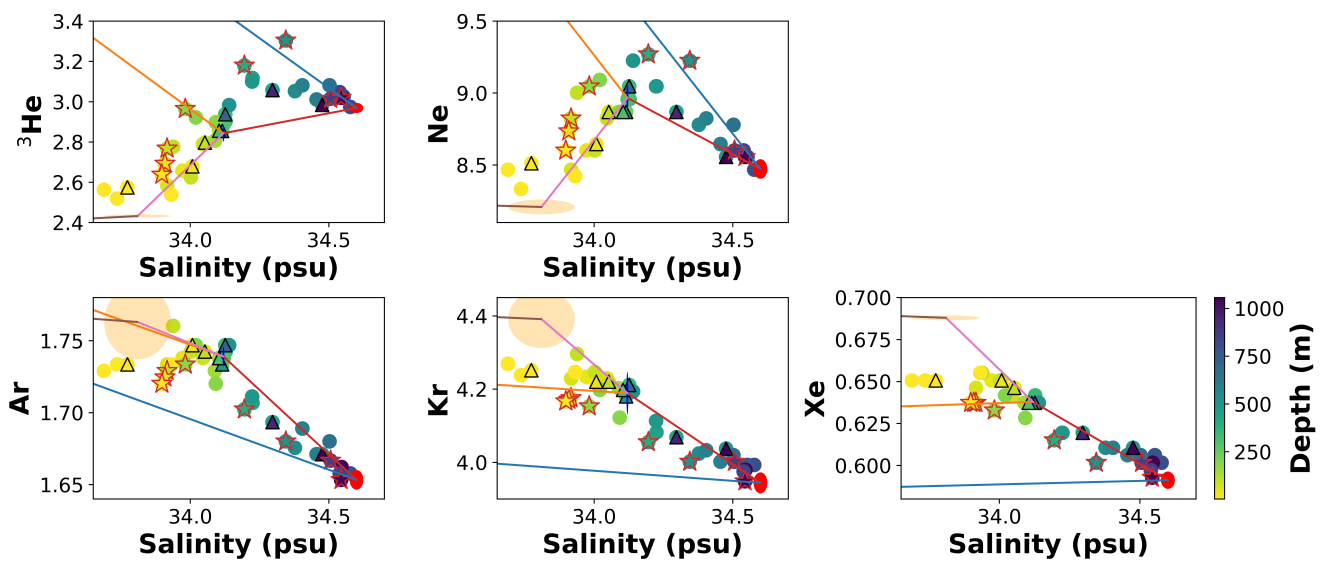


Figure S1. Diagrams of noble gases vs. salinity. The mixing lines between AASW and WW (pink lines) appear to be necessary to explain many values from the depths <200 m.

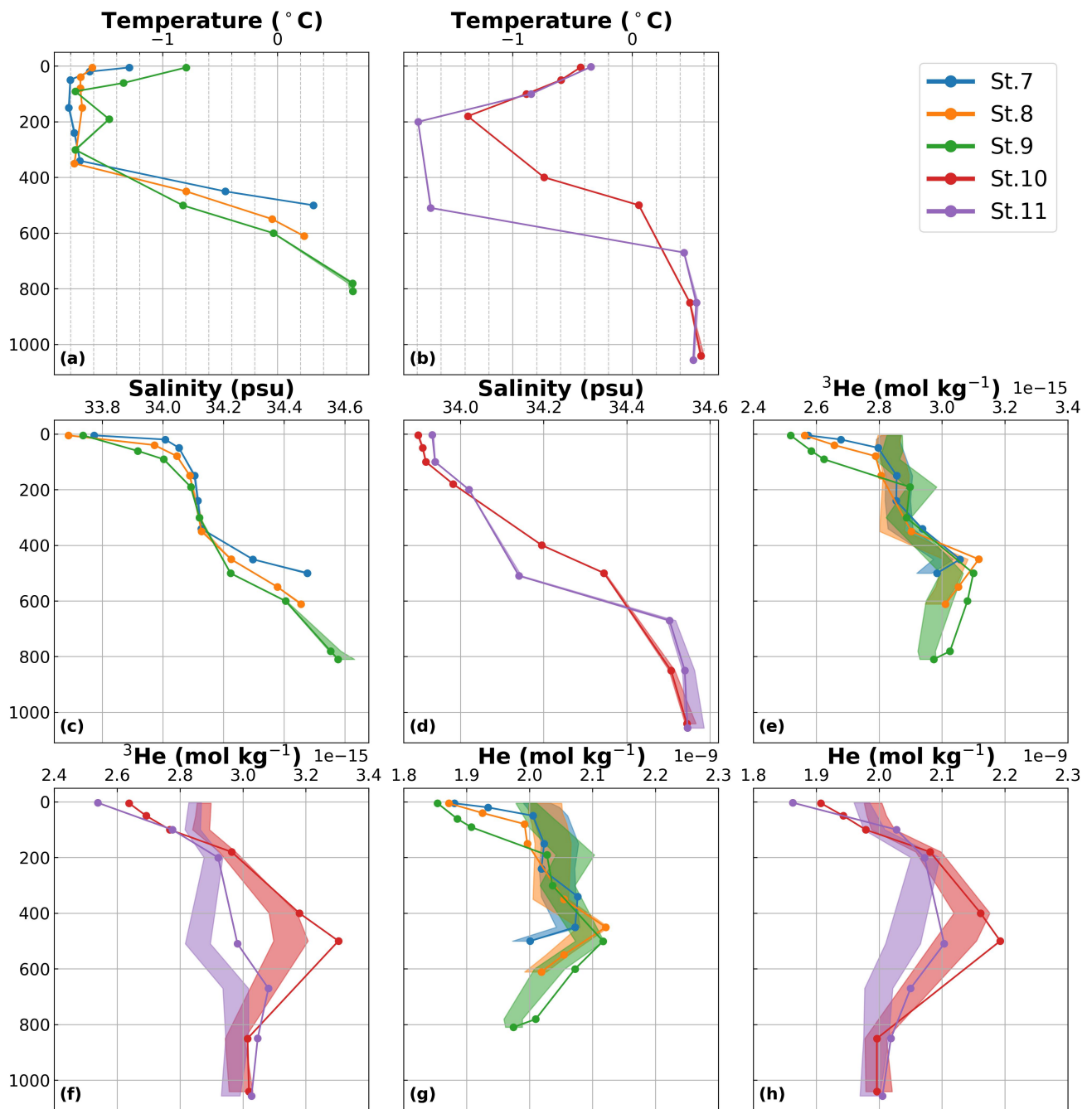


Figure S2. Comparison of the tracer profiles between the observed and reconstructed from the NG-OMPA results. (a, b) Potential temperature, (c, d) salinity, and (e-h) concentrations of He isotopes (^3He and ^4He). The profiles of the observed values are depicted in lines with dots. The reconstructed profiles are shown in shaded envelopes of mean and standard deviation of 10,000 profiles of the Monte Carlo simulation.

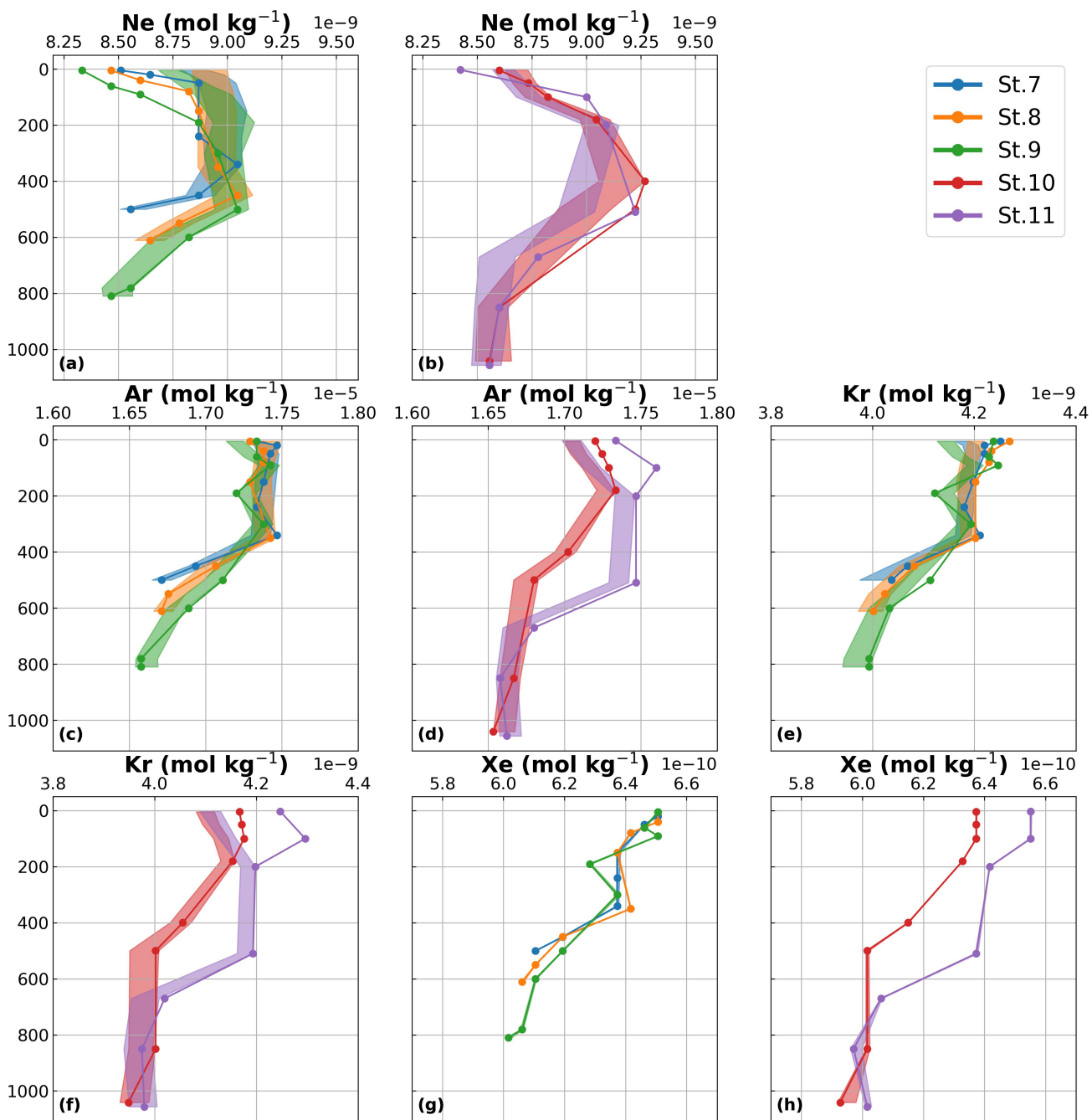


Figure S3. Comparison of the tracer profiles between the observed and reconstructed from the NG-OMPA results. The profiles of the observed values are depicted in lines with dots. The reconstructed profiles are shown in shaded envelopes of mean and standard deviation of 10,000 profiles of the Monte Carlo simulation.

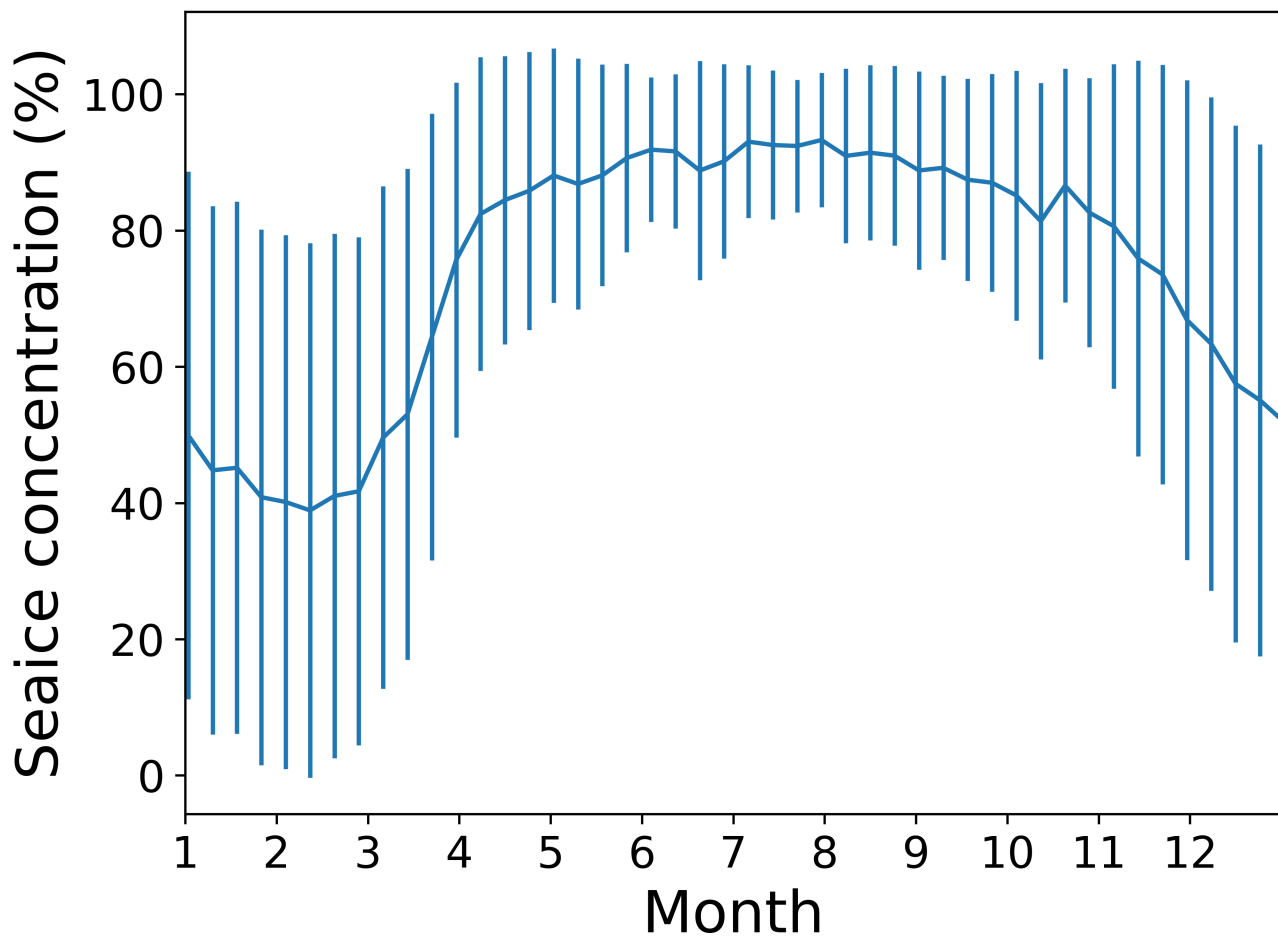


Figure S4. Seasonal variation of climatological sea ice concentration (2003 – 2018) in the Dotson Trough. The average concentrations of 8 days in the Dotson Trough were calculated from daily sea ice concentrations observed by AMSR-E and AMSR2 (Spreen et al., 2008). The highest concentrations are maintained from April to August until the concentrations slowly decrease from September.

REFERENCES

- Jenkins, A., Shoosmith, D., Dutrieux, P., Jacobs, S., Kim, T. W., Lee, S. H., et al. (2018). West Antarctic Ice Sheet retreat in the Amundsen Sea driven by decadal oceanic variability. *Nature Geosci* 11, 733–738
- Meredith, M. P., Brandon, M. A., Wallace, M. I., Clarke, A., Leng, M. J., Renfrew, I. A., et al. (2008). Variability in the freshwater balance of northern Marguerite Bay, Antarctic Peninsula: Results from $\delta^{18}\text{O}$. *Deep-Sea Research Part II-Topical Studies In Oceanography* 55, 309–322
- Östlund, H. G. and Hut, G. (1984). Arctic Ocean water mass balance from isotope data. *Journal Of Geophysical Research-Oceans* 89, 6373–10
- Randall-Goodwin, E., Meredith, M. P., Jenkins, A., Yager, P. L., Sherrell, R. M., Abrahamsen, E. P., et al. (2015). Freshwater distributions and water mass structure in the Amundsen Sea Polynya region, Antarctica. *Elementa: Science of the Anthropocene* 3, 000065–22
- Spreen, G., Kaleschke, L., and Heygster, G. (2008). Sea ice remote sensing using AMSR-E 89 GHz channels. *Journal of Geophysical Research* 113, C02S03